Measurement 235 (2024) 114931

Contents lists available at ScienceDirect

Measurement

journal homepage: www.elsevier.com/locate/measurement

Skyline force estimation and limitation during cable yarding: A novel technical solution for within the carriage

Stefan Leitner [a], Giovanni Carabin [a], Raffaele Spinelli [b], Massimiliano Renzi [a], Renato Vidoni [a,*]

[a] Faculty of Engineering, Free University of Bozen-Bolzano, UniBZ, Piazza Università 1, Province of Bolzano, I-39100, BZ, Italy
[b] Consiglio Nazionale delle Richerche-Istituto per la BioEconomia, CNR IBE, Via Madonna del Piano 10, Sesto Fiorentino, I-50019, FI, Italy

ARTICLE INFO

Keywords:
Agro-forestry mechatronics
Cable tension
Measurement
Estimation technique
Safety
Preventive maintenance

ABSTRACT

Forest operations are one of the most dangerous jobs in all fields of industrial production. Studies have shown that cable logging accidents are frequently caused by inadequate safety factors. Due to the limited reliability of theoretical models of cableway installations and the inefficacy of load limiters of existing machines, technical solutions for continuous skyline tensile force monitoring should be developed. This work proposes a novel concept and model to determine the skyline tensile force in real time, based on a non-invasive measurement and evaluation system built into the carriage. This information can be harnessed to improve the logging operational safety automatically and dynamically. The concept was tested with the help of a miniature cableway setup. The mean absolute error between the predicted and measured skyline tension for a total of 55 measurements was 14 %, and the maximum error was 29 %. This confirms the validity of the proposed approach.

1. Introduction and background

Being competitive in alpine logging operations requires being efficient. This demands quick cableway setup and dismantling, high productivity (fast movement and high payload), low operating cost during extraction and simple relocation to the subsequent felling site [1]. The pressure to perform may, however, come at the expense of safety. Forest operations are one of the most dangerous jobs in all fields of industrial production [2]. Varch et al. [3] concluded that the degree of mechanization and automation in logging operations is key to reduce risks. A study by Klun et al. [4] points to the importance of education, training, protection and improvement of personal safety equipment, technological development, organization and implementation in forest work.

Based on a study by Allman et al. [5], the most hazardous operation of logging operations is cable yarding. An analysis of accidents during cable yarding operations of Austria's largest forest enterprise ÖBf AG between 1998–2008 [6] showed that most accidents (63.2%) were caused by broken spar and anchor trees, bouncing cables and falling objects. The difficulty of giving a direct, sufficiently accurate and non-site-specific prediction of anchor tree load carrying capacities was confirmed in study [7]. The failure of cables and anchor trees was analyzed in measurement campaigns and compared with simulated data in [8,9], which also confirmed the difficulty to accurately predict the tension applied to the skyline. Other works monitored skyline tensile forces in cable logging, and compared the results with software calculations [10]. While most software solutions only rely on inaccurate static models, Mologni et al. [11] showed that finite element models could be successfully used for accurate and detailed analysis and simulation of the skyline tensile forces, including the dynamic oscillations due to the motion of the carriage and payload along the cable line. Based on study [12], in 55% of the work cycles, safe skyline force limits are exceeded, with the highest peaks often being caused at break-out during lateral skid. Dynamic factors during inhaul also frequently lead to unsafe skyline forces. Mologni et al. [12] state that operators often underestimate effects such as pretension, payload, and cable line geometry on skyline tensile forces. They further state that, due to the limited reliability of theoretical models and the inefficacy of load limiters of existing machines, technical solutions for continuous skyline tensile force monitoring should be adopted.

Cable tension force estimation techniques based on integrated vision and inertial measurement systems [13], vision-based vibration analysis [14], acoustic pressure signals [15] and microwave remote sensing [16], among others, have been proposed for applications such as bridges and roofs. These concepts are, however, not adequate for largely diverse and mobile installations such as cable logging setups. In this work, concepts to enable the determination of the skyline tensile force in real time, based on a non-invasive measurement and evaluation system mounted directly on the carriage are proposed. Based on this data, dropline- and self-propelled carriages could automatically and

* Corresponding author.
E-mail address: renato.vidoni@unibz.it (R. Vidoni).

https://doi.org/10.1016/j.measurement.2024.114931
Received 30 October 2023; Received in revised form 8 February 2024; Accepted 16 May 2024
Available online 21 May 2024

dynamically limit the force of the dropline to keep skyline tensile forces within safe limits, especially during lateral skid. Self-propelled carriages can also be programmed to automatically limit driving speed to lower the impact of dynamic effects, or to come to a complete stop, if skyline force limits are exceeded during the inhaul phase. For example, this could be the case when approaching the middle of a large span. When working with non-motorized carriages, or during the inhaul phase with dropline carriages, the skyline tensile force estimate can be forwarded to the tower yarder or sled winch to achieve the same level of automated safety. Finally, the continuous skyline tensile force profile can also be logged for skyline predictive maintenance purposes, among others.

The paper provides several contributions: First, it proposes six concepts in total on how to estimate the skyline force within a cable logging carriage, based on different sets of sensors. Second, for each concept, the number, type and mounting position of the sensors is discussed. Third, analytical evaluations are performed and discussion is provided to study the accuracy, limitations and applicability of each concept. Fourth, design considerations are provided for the selection of the best concept for various types of carriages. The proposed concepts can therefore cover a wider range of applications and arrangements in tensile strength analysis of cable yarding applications and can overcome the current limitations of the models available in literature. In particular, and unlike existing solutions, the concepts do not rely on introducing cable deflection or on inserting measurement devices into the cable path, but rely solely on passive and non-invasive measurement methods.

The organization of the paper is as follows: Section 2 develops the main concepts behind the estimation of the skyline tensile force within the carriage. Sections 2.1 to 2.4 describe respectively the governing mathematical models, model accuracy, limitations of the concept, as well as several variations providing different degrees of applicability. Section 3.1 describes the miniature cableway installed to validate the proposed concepts. The data acquisition procedure and test results are presented in Section 3.2. Findings are discussed in Section 4 and the work is concluded in Section 5.

2. Concept development

2.1. Modeling

This section develops the most general model of how the force on the skyline can be determined given a set of data attainable within the carriage suspended on the skyline. Table 1 lists all variables used in the subsequent derivations.

Fig. 1 shows a carriage carrier module, consisting of two pulleys in a tandem setup. The sub-indexes f of all reported variables in the figures and equations indicate association with the carrier module on the front side of the carriage. Similarly, sub-indexes r are associated with the rear side carrier module (Fig. 2). Due to the symmetry of the carrier modules, and nearly identical forces (F_S) in the skyline on both sides of the carrier modules, it follows that the curvature (δ_f and δ_r) of the skyline must be equal on both pulleys of the same carrier module. In other words, force equilibrium among both pulleys of a carrier module is reached, when the carrier module tilts to the angle which results in balanced curvature of the skyline. Given this observation, the total radial force F_{P_f} and F_{P_r} per pulley can be computed as follows:

$$F_{P_{f,r}} = \sqrt{2 \cdot F_S^2 \cdot [1 - cos(\delta_{f,r})]} \tag{1}$$

Again, due to constant F_S, F_{P_f} and F_{P_r} point in the direction that divides the curvature angle. That is, respectively, $\frac{\delta_f}{2}$ and $\frac{\delta_r}{2}$ short of perpendicular to the section of skyline cable extending between the two pulleys of a carrier module, as indicated in Fig. 1. The vertical

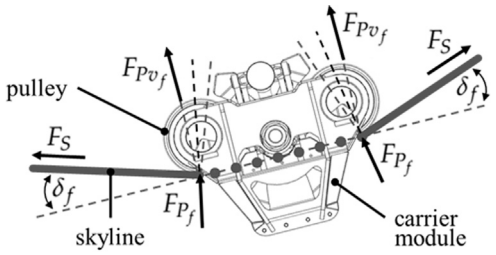

Fig. 1. Free body diagram of a carriages' carrier module.

force components F_{Pv_f} and F_{Pv_r} (based on coordinate systems defined by the carrier modules themselves) on the pulleys are thus given by:

$$F_{Pv_{f,r}} = F_{P_{f,r}} \cdot cos\left(\frac{\delta_{f,r}}{2}\right) \tag{2}$$

It should be noted that by observation of Fig. 1 or by using the trigonometric identity $cos^2\left(\frac{\delta_{f,r}}{2}\right) = \frac{1+cos(\delta_{f,r})}{2}$, Eqs. (1) and (2) can be simplified to:

$$F_{Pv_{f,r}} = F_S \cdot sin\left(\delta_{f,r}\right) \tag{3}$$

Eqs. (1) and (2) are still helpful, for example if the estimation of F_S is to be based on a measurement of $F_{P_{f,r}}$. Subsequent calculations will therefore be based on this most general representation. Fig. 2 depicts both the frontal and rear carrier modules, and the main body of the carriage. Based on the inclinations β_f and β_r of the carrier modules with respect to the carriages' body, which in turn is inclined by α, the vertical force components F_{Cy_f} and F_{Cy_r} of the carrier modules contributing to the suspension of the carriage are given by:

$$F_{Cy_{f,r}} = 2 \cdot F_{Pv_{f,r}} \cdot cos(\beta_{f,r}) \tag{4}$$

It must be noted that Eq. (4) is only accurate if the centers of the pulleys and the pivot point of the carrier module are perfectly in line. In the example of Fig. 1, the pivot point is below the line connecting the centers of the pulleys. This asymmetrical positioning must be compensated by unequal forces at the two pulleys of the module, brought about by asymmetrical skyline curvature. This results in a force which counteracts rotation of the tandem module, resulting in smaller $\beta_{f,r}$. Smaller $\beta_{f,r}$ at a given load condition ultimately leads to a slight overestimation of F_S. Assuming alignment of pulleys and the pivot point, force equilibrium yields that the sum of F_{Cy_f} and F_{Cy_r} must support all force components in the direction perpendicular to a plane P_α, where P_α is inclined from the horizontal plane by α. It follows that:

$$F_{Cy_f} + F_{Cy_r} = \left(m_C \cdot g + F_D\right) \cdot cos(\alpha), \tag{5}$$

where m_C is the mass of the carriage, g is the gravitational acceleration and F_D is the force in the dropline cable. Solving Eqs. (1) to (5) for F_S yields two possible representations of F_S, Eqs. (6) and (7) given in Box I:

In a practical application, m_C can be predetermined, while F_D, α, β_f and β_r can be measured in real time via sensors within the carriage. Fig. 3 provides more details of this set of sensors, their type, their installation location within the carriage and the physical signal they measure.

The procedure that follows describes how δ_f and δ_r can be expressed as a function of the carriages' geometry and β_f and β_r. Eq. (6) thus provides an explicit expression for the computation of the skyline force in real time, based on only four variables to be measured by sensors within the carriage.

For the computation of δ_f and δ_r, one must consider Fig. 4, which shows the relationship between δ_f and β_f, and δ_r and β_r, which is given by:

$$\delta_f = \beta_f + \gamma \tag{8}$$

Table 1
Legend of variables of the subsequent derivations.

Var.	Unit	Definition
α	°	Inclination angle of the carriages' main body
β_f	°	Front carrier module tilting angle with respect to the carriages' main body
β_r	°	Rear carrier module tilting angle with respect to the carriages' main body
γ	°	Inclination angle of skyline cable section between the two inner pulleys of the carrier modules with respect to the carriages' main body
δ_f	°	Curvature of the skyline cable per pulley on front carrier module
δ_r	°	Curvature of the skyline cable per pulley on rear carrier module
F_S	N	Skyline cable force
F_{P_f}	N	Total force on each pulley of the front carrier module
F_{P_r}	N	Total force on each pulley of the rear carrier module
F_{Pv_f}	N	Vertical force component on each pulley of the front carrier module
F_{Pv_r}	N	Vertical force component on each pulley of the rear carrier module
F_{Cy_f}	N	Force component of the front carrier module in y direction
F_{Cy_r}	N	Force component of the rear carrier module in y direction
F_D	N	Dropline cable force
F_{bx}	N	Force measured with sensor (load cell) labeled as bx in Figs. 5 and 6
m_C	kg	Mass of the carriage
ΔPv_f	mm	Front carrier module inner pulley vertical shift due to tilt β_f
ΔPv_r	mm	Rear carrier module inner pulley vertical shift due to tilt β_r
ΔPh_f	mm	Front carrier module inner pulley horizontal shift due to tilt β_f
ΔPh_r	mm	Rear carrier module inner pulley horizontal shift due to tilt β_r
FL_{ratio}	–	Ratio of F_S and the total load suspended by the skyline
ΔF_S	%, N	Error of F_S
$\Delta F_{S_{m_C}}$	%, N	Error of computed F_S due to inaccurate m_C estimate
$\Delta F_{S_{F_D}}$	%, N	Error of computed F_S due to inaccurate F_D measure
ΔF_{S_α}	%, N	Error of computed F_S due to inaccurate α measure
ΔF_{S_β}	%, N	Error of computed F_S due to inaccurate β measure
$\Delta F_{S_{bx}}$	%, N	Error of computed F_S due to inaccurate F_{bx} measure
Δm_C	%, kg	Error in computing or measuring m_C
ΔF_D	%, N	Error in measuring F_D
$\Delta\alpha$	%, °	Error in measuring α
$\Delta\beta$	%, °	Error in measuring β
ΔF_{bx}	%, N	Error in measuring F_{bx}
D	mm	Center distance of the inner two pulleys of the front and rear carrier modules when $\beta_f = \beta_r = 0$
L	mm	Distance between the center of a carrier modules' pulley and the pivotal axis of the tandem carrier module

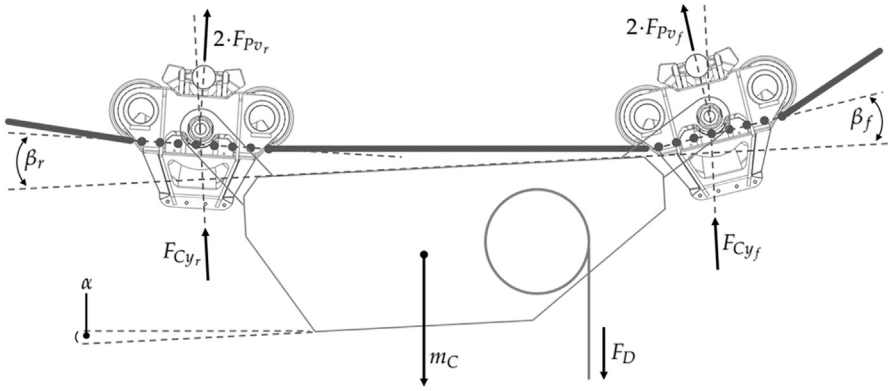

Fig. 2. Forces acting on the carrier modules and main body of a carriage. Mainline (and haulback) cables are not shown.

$$F_S = \frac{\left(m_C \cdot g + F_D\right) \cdot cos(\alpha)}{2 \cdot \sqrt{2 \cdot [1 - cos(\delta_f)]} \cdot cos\left(\frac{\delta_f}{2}\right) \cdot cos(\beta_f) + 2 \cdot \sqrt{2 \cdot [1 - cos(\delta_r)]} \cdot cos\left(\frac{\delta_r}{2}\right) \cdot cos(\beta_r)} \tag{6}$$

$$F_S = \frac{\left(m_C \cdot g + F_D\right) \cdot cos(\alpha)}{2 \cdot sin(\delta_f) \cdot cos(\beta_f) + 2 \cdot sin(\delta_r) \cdot cos(\beta_r)} \tag{7}$$

Box I.

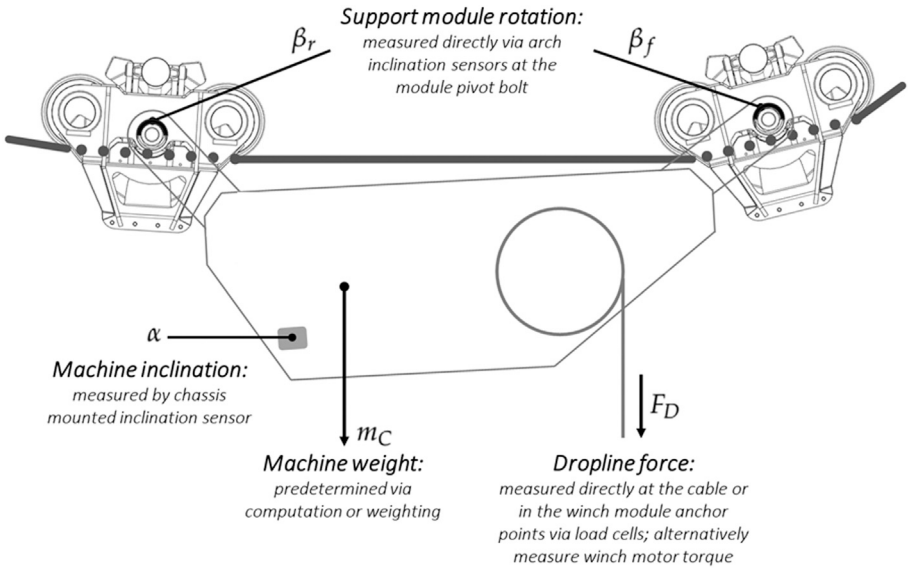

Fig. 3. Set of sensors to determine the skyline force based on the concept described by Eq. (6).

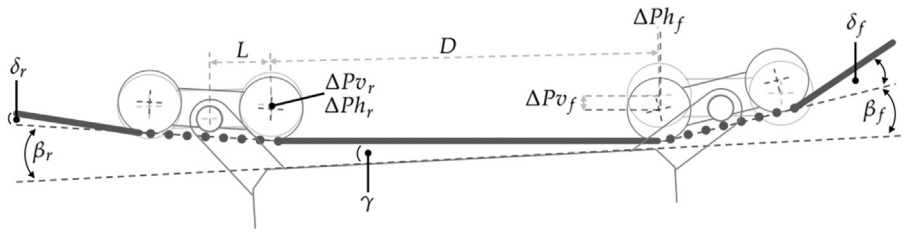

Fig. 4. Visualization of how the carriage geometry and carriage module inclinations influence the skyline curvature.

$$\delta_r = \beta_r - \gamma, \tag{9}$$

where γ is the angle between the carriages' body and the section of skyline cable extending between the inner pulleys of the front and rear carrier modules. This definition assumes that the carrier modules are mounted at an equal height with respect to the main body of the carriage. That is, if the skyline did not have any curvature (perfectly straight line), γ would take on a value of zero. This is a reasonable assumption based on the observation of existing solutions on the market.

Rotations β_f and β_r of the carrier modules lead to a vertical (ΔPv_f, ΔPv_r) and horizontal (ΔPh_f, ΔPh_r) shift of the contact points between skyline cable and carrier pulleys, as indicated in Fig. 4 and computed as follows:

$$\Delta Pv_{f,r} = L \cdot sin(\beta_{f,r}) \tag{10}$$

$$\Delta Ph_{f,r} = L \cdot [1 - cos(\beta_{f,r})] \tag{11}$$

Eqs. (10) and (11) describe the vertical and horizontal shift of the lowest point (or center) of the pulleys. With $\beta_f = \beta_r$, implying $\gamma = 0$, these would indeed be the contact points of interest between skyline cable and pulley, precisely vertically below the center of the pulleys. With $\beta_f <> \beta_r$, and therefore $\gamma <> 0$, the contact points shift along the tangential curve of the pulleys. Since all pulleys are identical, this shift has no impact on γ, which can therefore be computed as follows:

$$tan(\gamma) = \frac{\Delta Pv_f - \Delta Pv_r}{D + \Delta Ph_f + \Delta Ph_r} \tag{12}$$

Finally, from Eqs. (8) to (12), δ_f and δ_r follow as:

$$\delta_f = \beta_f + tan^{-1}\left\{ \frac{L \cdot [sin(\beta_f) - sin(\beta_r)]}{D + L \cdot [2 - cos(\beta_f) - cos(\beta_r)]} \right\} \tag{13}$$

$$\delta_r = \beta_r - tan^{-1}\left\{ \frac{L \cdot [sin(\beta_f) - sin(\beta_r)]}{D + L \cdot [2 - cos(\beta_f) - cos(\beta_r)]} \right\} \tag{14}$$

2.2. Accuracy and sensitivity

The model presented estimates the force within the skyline based on its degree of deflection given a load on the skyline in the direction of gravity. In a prior study [11], a total load of 35 kN on the skyline resulted in the skyline force exceeding 223 kN. The skyline force to skyline loading ratio (FL_{ratio}), defined here by the inverse of the denominator of Eq. (6), was thus at least 6.37. Values of 4 to 8 seem common for FL_{ratio}. This shows that F_S computed via Eq. (6) is very sensitive with respect to the accuracy of its input variables m_C, F_D, α, β_f and β_r.

Total carriage mass m_C can be predetermined. To improve the accuracy, mass variations due to varying amounts of fuel in the tank or variable amounts of cable on the winch drum can be compensated by introducing a fuel level sensor and tracking winch activity, respectively. This should allow for the determination of carriage mass with at most a few kilograms of error. This error amplifies with a factor of $FL_{ratio} \cdot cos(\alpha) \cdot g$ into F_S, resulting in an error in the order of a few kN or less.

Winch force F_D can be determined via load cells, or computed by monitoring the torque of the winch motor (in motorized carriages). The latter approach may however suffer significant inaccuracy, as the effective radius of a drum based winch varies with the amount of cable on the drum and the way the cable is wound onto the drum. In either case, an error in the order of a few kN is likely unavoidable. Further it is assumed that the load is fully suspended, such that the direction of force vector F_D is known. This limitation is discussed in Section 2.3. The error of F_D is also amplified by $FL_{ratio} \cdot cos(\alpha)$, likely resulting in significant error.

Table 2
FL_{ratio} as a function of β and F_S percentage error ($\Delta F_{S_\beta}(\beta, \Delta\beta)$) as a function of β and $\Delta\beta$.

β (°)	0.5	1.0	1.5	2.0	3.0	5.0	7.5	10.0	15.0
FL_{ratio} [Eq. (16)]	28.6	14.3	9.6	7.2	4.8	2.9	1.9	1.5	1.0
$\Delta F_{S_\beta}(\Delta\beta = 0.02°)$ [Eq. (18)]	0.40	0.20	0.13	0.10	0.07	0.04	0.03	0.02	0.01
$\Delta F_{S_\beta}(\Delta\beta = 0.04°)$ [Eq. (18)]	0.80	0.40	0.27	0.20	0.13	0.08	0.05	0.04	0.03
$\Delta F_{S_\beta}(\Delta\beta = 0.08°)$ [Eq. (18)]	1.60	0.80	0.53	0.40	0.27	0.16	0.11	0.08	0.05

Crane inclination α can be determined via a dedicated inclination sensor. With a sensing range of ±45°, a total sensor-control unit resolution of 10 bits far outperforms a common sensor accuracy of ±0.5°. The sensitivity of F_S on α can be found by differentiating Eq. (6) with respect to α, yielding $\frac{dF_{S_\alpha}}{d\alpha} \propto -sin(\alpha)$. The larger the inclination (identical in decline), the larger the impact of sensor inaccuracy. The error is thus as large as:

$$\Delta F_{S_\alpha}(\alpha = 45°, \Delta\alpha = \pm 0.5°) = \frac{sin(45°) \cdot \frac{\pm 0.5° \cdot \pi}{180°}}{cos(45°)} = \pm 0.88\%, \tag{15}$$

or equal to ± 2.2 kN at an F_S of 250 kN.

β_f and β_r, together with crane geometrical constants D and L, fully determine FL_{ratio}. Since F_S is very sensitive to FL_{ratio}, and since β_f and β_r are generally very small (few degrees), β_f and β_r must be measured very accurately, possibly via dedicated sensors at the carrier modules. Sensor resolution can be increased by minimizing sensing range. When the crane is suspended and not placed at a skyline support, β_f and β_r must by definition be larger than zero. A sensing range of 0°−40° should thus be more than sufficient. With a total sensing resolution of 10 bits and a non-linearity of ±0.5%, the error should be no larger than 0.04° at a β_f or β_r of less than about 8°. With increasing β_f and β_r, sensing accuracy becomes less critical, since FL_{ratio} becomes small. To perform sensitivity analysis, consider the simplified case where $\beta_f = \beta_r$. From Eqs. (13) and (14) follows that $\beta_f = \beta_r = \delta_f = \delta_r = \beta$. Since β is small, Eq. (6) approximates to, and yields sensitivity analysis, respectively:

$$F_S \propto FL_{ratio} = \frac{1}{4 \cdot \sqrt{2 \cdot [1 - cos(\beta)]} \cdot cos\left(\frac{\beta}{2}\right) \cdot cos(\beta)} \approx \frac{1}{4 \cdot \sqrt{2 \cdot [1 - cos(\beta)]}} \tag{16}$$

$$\frac{dF_{S_\beta}}{d\beta} \propto -\frac{sin(\beta)}{8 \cdot \sqrt{2} \cdot (1 - cos(\beta))^{\frac{3}{2}}} \tag{17}$$

For a given β, the percentage error in F_S is thus given by:

$$\Delta F_{S_\beta}(\beta, \Delta\beta) \approx -\frac{\frac{sin(\beta)}{8 \cdot \sqrt{2} \cdot (1 - cos(\beta))^{\frac{3}{2}}}}{\frac{1}{4 \cdot \sqrt{2 \cdot [1 - cos(\beta)]}}} \cdot \Delta\beta = \frac{sin(\beta)}{2 \cdot (cos(\beta) - 1)} \cdot \Delta\beta \tag{18}$$

Given values of 6.28 and 8 for FL_{ratio} in previous studies, Table 2 shows that common values for β_f and β_r are in the range of 1.5° and 2.5°. With a sensor resolution of 0.04°, the error of F_S is limited to less than 0.27%, or ± 675 N at an F_S of 250 kN. For consistency purposes, it should be noted that $FL_{ratio}(\beta = 15°) = 1$. This because the skyline exiting the carriage at an angle of 30° supports 50% of its mass per side. Similarly, $FL_{ratio}(\beta = 45°) = 0.5$, as the carriage is perfectly suspended by two vertical sections of the skyline, in which case F_S takes on its minimum value.

Table 3 provides a summary and a quantitative overview of all main sources of error when computing F_S. Not reported and not considered in the model are parasitic mechanical effects, such as for example the resistance of the skyline against being bent around the carriers' pulleys. Such effects are thought to only have a very small impact on the computed result, but practical investigations would have to be made to confirm this. Of the sources of error studied, the difficulty to accurately determine F_D appears to be by far the largest contributor to $\Delta F_S = \Delta F_{S_{m_C}} + \Delta F_{S_{F_D}} + \Delta F_{S_\alpha} + \Delta F_{S_\beta}$.

Table 3
Summary, overview and quantification of all sources of error in determining F_S.

Source of error	Error quantification	Comments
$\Delta F_{S_{m_C}}$	$FL_{ratio} \cdot cos(\alpha) \cdot g \cdot \Delta m_C$	Likely less than 1 kN (≪1%)
$\Delta F_{S_{F_D}}$	$FL_{ratio} \cdot cos(\alpha) \cdot \Delta F_D$	Likely at least several kN (≫1%)
ΔF_{S_α}	$FL_{ratio} \cdot (m_C \cdot g + F_D) \cdot sin(\alpha) \cdot \Delta\alpha$	At most a few kN (<1%)
ΔF_{S_β}	$-\frac{sin(\beta) \cdot (m_C \cdot g + F_D) \cdot cos(\alpha)}{8 \cdot \sqrt{2} \cdot (1 - cos(\beta))^{\frac{3}{2}}} \cdot \Delta\beta$	Very small at small FL_{ratio} (<1%)

2.3. Limitations

There are several conditions, under which the determination of F_S employing the concept described in the previous sections is not possible. These conditions are as follows:

1. Carriage is not fully suspended: If the carriage is not fully suspended, it is unclear how much loading leads to the support module inclinations β_f and β_r measured.
2. Carriage is positioned at a skyline support unit: If at least one of the carriages' carrier modules is on top of a skyline support, or if the skyline support is located in between the carriages' carrier modules, the section of skyline cable observable via on-board sensors takes on a concave shape. In that case, by definition, β_f and β_r take on negative values. This condition can be used as indicator of the presence of a skyline support, at which point F_S cannot be determined. In addition, since the skyline support itself carries most of the carriages' load, F_S should take on a minimum value under this condition. The inability to determine F_S should thus have no safety implications.
3. Load is not fully suspended: Apart from accurate F_D measurement, the direction of this force vector is of paramount importance. Eqs. (5) and (6) assume full load suspension, such that the vector of F_D points in the direction of gravity. In the case of partial suspension, or during lateral yarding, it is unknown what percentage of measured F_D contributes to load on the skyline, and what percentage of F_D translates to force in the mainline (or haulback) cable. Actual F_S may thus be much smaller than predicted.
4. Mainline (and/or haulback) cables are not parallel to the skyline: If the mainline and/or haulback cables are not parallel to the skyline, they contain a force component adding to or subtracting from the total load suspended on the skyline, but not captured by the described approach. This is the case in particular when getting close to a support unit.
5. Dynamic effects are largely ignored or lead to erroneous results: radical load changes, such as break-out events during lateral yarding or carriage acceleration induce oscillations into the skyline. This leads to the skyline and carriage oscillating up and down for up to several meters, especially on longer cableways. In the unloaded case, skyline loading equals m_C. At the lowest point of oscillation, β_f and β_r are maximized, minimizing FL_{ratio} and thus F_S. In reality F_S takes on its maximum value at the lowest point of oscillation. The opposite is true at the highest point of oscillation. β_f and β_r are minimized, maximizing FL_{ratio} and thus F_S, despite actual F_S being minimized.

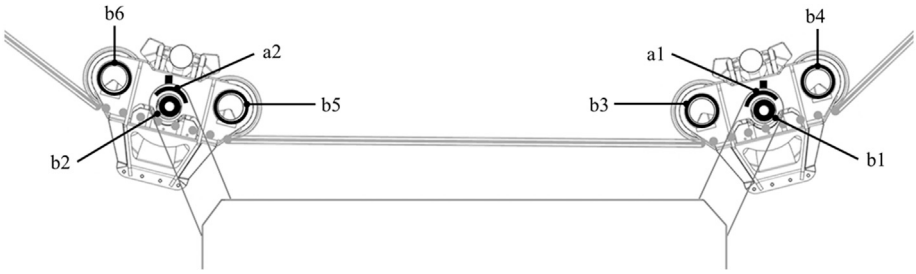

Fig. 5. Possible installation locations of sensors within the carrier modules.

Table 4
Sensor options to support the estimation of F_S.

Label	Physical value measured —sensor type	Variable measured
a1, a2	Carrier inclination —angular inclination sensor	β_f and β_r, resp.
b1, b2	Lift component of carrier module force —load cell	F_{Cy_f} and F_{Cy_r}, resp.
b3, b4	Total force per pulley on the front carrier module —load cell	F_{Pv_f}
b5, b6	Total force per pulley on the front carrier module —load cell	F_{Pv_r}
b7	Lift force on the single front carrier pulley—load cell	$F_{Cy_f} = F_{Pv_f}$
a3	Skyline curvature per pulley on the front carrier module —angular inclination sensor	δ_f

6. The concept determines the force in the skyline at the current location of the carriage (and not at a skyline anchor point or the point of maximum skyline force): The estimation of F_S is based on the curvature of the skyline at the carriage's support units, given the load of the carriage on the skyline (true for all concepts presented in this work). F_S is therefore an estimate of the skyline force at the current location of the carriage. When the carriage moves along the cableway, it can keep track of skyline inclination and length. Given the load per unit length on the skyline cable (mass of the cable itself), cable suspension theory can be used to approximate the cable force at the highest point of the cableway, projecting from the current location of the carriage.
7. Carriage traction force may need to be considered: some self-propelled carriages, such as the Woodliner by Konrad (Konrad Forsttechnik GmbH, Preitenegg, Austria -www.forsttechnik.at/en/) or the Tecno Series by Greifenberg (Greifenberg Teleferiche Sas, Terzolas, Italy - www.greifenberg.it/) use the skyline cable itself for traction. Depending on the direction of the traction force and the exact combination and setup of sensors used, the traction force may need to be added to the estimated F_S.

2.4. Variations and applicability

The inability to accurately determine the total load suspended by the skyline, in particular due to an error in determining F_D (sources of error $\Delta F_{S_{m_C}}$, $\Delta F_{S_{F_D}}$ and ΔF_{S_α}, according to Table 3) significantly lowers the accuracy of the proposed concept. In addition, this is also responsible for limitations 1, 3, 4 and 5 described in Section 2.3. Overcoming this shortcoming significantly improves the accuracy of this approach and limits its unavailability to the small sections at support units (limitation 2 described in Section 2.3), which, as discussed, are instances where F_S is minimized and thus uncritical.

What follow in Table 5 are different approaches to overcome those limitations, based on different sets of additional sensors and thus in part at the expense of additional hardware. Table 4 lists additional sensors that could be considered, as indicated in Figs. 5, 6 and 7. Also mentioned are the sensor types and the physical values they measure.

It should be noted that due to the symmetry of the carrier modules, b3, b4 and b5, b6 measure the same value. With the help of Eqs. (4) follows that:

$$F_{b3} = F_{b4} = F_{Pv_f} = \frac{F_{Cy_f}}{2 \cdot \cos \beta_f} \tag{19}$$

$$F_{b5} = F_{b6} = F_{Pv_r} = \frac{F_{Cy_r}}{2 \cdot \cos \beta_r} \tag{20}$$

Unlike concept A, concepts B to E do not rely on measurements of m_C, F_D and α. Thus $\Delta F_{S_{m_C}}$, $\Delta F_{S_{F_D}}$ and ΔF_{S_α} are replaced by:

$$\Delta F_{S_{b_x}} = FL_{ratio} \cdot \Delta F_{bx}, \tag{22}$$

for one or more x $\in \{1, 2, 3, 4, 5, 6\}$. Since F_{bx} is measured directly, it is fair to assume that ΔF_{bx} is less than 1%. For this reason, concepts B to E can be expected to significantly reduce ΔF_S. In addition, concepts B to E provide a valid measure under all circumstances, except when the carriage is located on top of a skyline support. Thus concept A has clear disadvantages compared to concepts B to E when it comes to the validity and accuracy of the force estimation, despite requiring a relatively large number of sensors. Concept A has been included for completeness, but would be a poor choice in an actual design.

If the carriage is small and does not have tandem skyline pulleys, or only a single tandem pulley on the front side, concepts F and D (or E) are respectively the simplest and most effective choices. In both cases, direct measurements of all data can be performed with two sensors only. In the latter case, D may be favorable over E, as it does not require the additional mechanics of an inclination wheel. Carriages with tandem carrier modules on the front and rear sides should make use of concepts B or C. Concept C allows direct measurement of all unknowns with three sensors, while concept B requires one additional sensor. The advantage of concept B with respect to C is added redundancy and possibly improved accuracy, as it can provide two almost independent force estimates. The estimation logic of concept B could deliver the average of both estimates if the error between them is small, while still provide a valid estimate if one sensor signal provides invalid data. This improved robustness however comes at an additional cost and has to be evaluated on a case by case bases.

The computational effort to estimate the skyline force is negligibly small, no matter the concept of choice. Common industrial machine controllers can process the set of expressions described in this work much faster than what would make sense from a physical standpoint. In practice it could make sense to implement a low pass filter to remove high frequency noise components in the skyline force estimate.

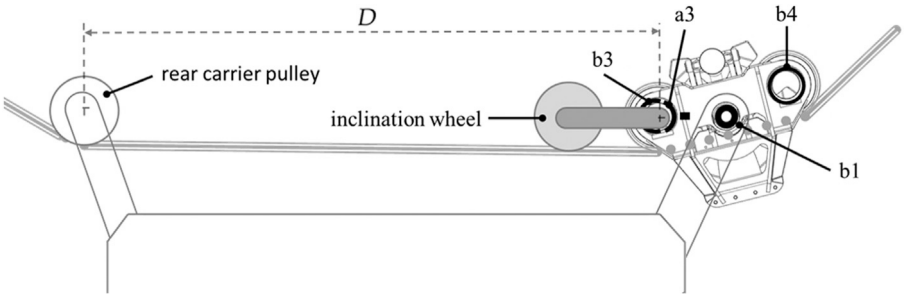

Fig. 6. Sensor options in combination with a single rear carrier pulley and inclination wheel measuring device.

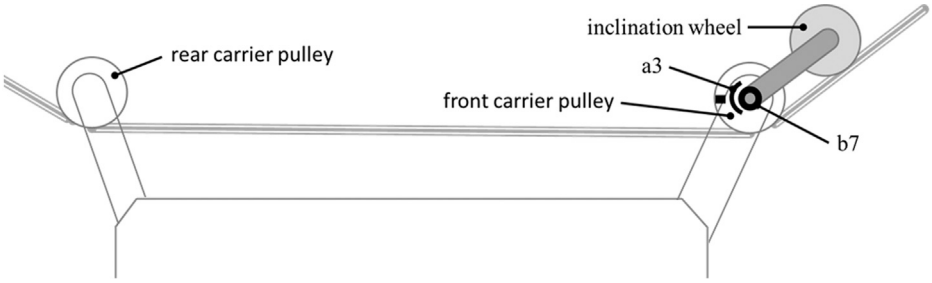

Fig. 7. Sensors on a carriage with single front and rear carrier pulleys and an inclination wheel measuring device.

Table 5
Concepts to determine the force in the skyline based on different sets of sensors.

#	Setup and set of sensors	Description	Modeling
A	**4+ sensors:** a1, a2, F_D sensing, α sensing (at least 4 sensors, additional sensors to boost accuracy)	Precision and applicability are limited by the inability to (accurately) determine m_C and F_D	Eqs. (1) to (14)
B	**4–6 sensors:** a1, a2, b1 or at least one of b3/b4, b2 or at least one of b5/b6 (at least 4 sensors)—Fig. 5	m_C and F_D are indirectly captured by measuring the total loading on the skyline at one or multiple points of the carrier modules	Eqs. (1) to (14) still hold, by eliminating m_C, F_D and α from Eq. (5) with the help of Eqs. (19) and (20). It is also possible to compute two separate values for F_S based on associating measurement F_{a1} and F_{a2} with forces having subscripts f and r, respectively—redundancy and improved accuracy
C	**3–4 sensors:** a1, a2, b1 or at least one of b3/b4 (at least 3 sensors)—Fig. 5	Equivalent to concept B, but based solely on the loading of the skyline at the frontal carrier module	Eqs. (1) to (14) still hold by eliminating m_C, F_D and α from Eq. (5) with the help of Eq. (19) and ignoring all forces associated with index r (the rear carrier module). Measurement a2 is still required to compute γ
D	**2–3 sensors:** Use of rear carrier pulley, a1, b1 or at least one of b3/b4 (at least 2 sensors)—Fig. 5	Compared to concept C, a2 is not required in case of a single rear carrier pulley (no tandem setup). The single carrier pulley serves as a fixed reference point, such that β_f and γ are fully determined via a1	Eqs. (1) to (14) still hold by eliminating m_C, F_D and α from Eq. (5) with the help of Eq. (19), by ignoring all forces associated with index r (the rear carrier module) and setting β_r to zero when computing γ with the help of Eqs. (10) to (12). This replaces the need to measure a2
E	**2–3 sensors:** Use of rear carrier pulley and inclination wheel, a3, b1 or at least one of b3/b4 (at least 2 sensors)—Fig. 6	The inclination wheel is capable of capturing total skyline curvature at the carrier pulley, directly determining δ_f. Since β_f is still required to compute F_S, the rear carrier cannot be a tandem setup	Eqs. (1) to (6) still hold by eliminating m_C, F_D and α from Eq. (5) with the help of Eq. (19), by ignoring all forces associated with index r (the rear carrier module). β_r is zero and δ_f is measured directly via a3, which yields β_f with the help of Eq. (13): $\delta_f = \beta_f + tan^{-}1\left\{\frac{L \cdot sin(\beta_f)}{D + L \cdot [1 - cos(\beta_f)]}\right\}$ (21) which can be easily solved numerically in real time.
F	**2 sensors:** Use of front and rear carrier pulley, and an inclination wheel, a3, b7 (2 sensors)—Fig. 7	Due to the fixed reference at the rear carrier pulley, the inclination wheel (a3) is capable of capturing total skyline curvature at the carrier pulley, directly determining δ_f. b7 measures F_{Cy_f}, which in this case by definition equals F_{Py_f}	$F_S = \frac{F_{Cy_f}}{sin(\delta_f)}$ $FL_{ratio} = \frac{1}{sin(\delta_f)}$

Fig. 8. Skyline tensile force observer test setup consisting of a wooden carriage with a loading platform suspended by a skyline.

Another aspect to be considered when selecting the set of sensors and their mounting positions on the carriage is overall system reliability, since cable logging often deals with harsh operating and weather conditions. All sensors and auxiliary mechanics must be able to deal with large temperature variations, ice formation and contaminants like grease and oils. The accuracy of the measurements should not be impacted significantly by minor wear in the pulleys or other mechanics. The design should also foresee robust protective covers for all sensitive parts.

3. Experimental setup and test results

3.1. Miniature cableway installation

The objective in this section is to validate the concept introduced in Section 2. The primary goal is not to test the accuracy of the skyline tensile force observer, but to conclude with reasonable confidence that no mistakes have been made in the problem formulation or any of the derivations.

To achieve this, a small scale wooden cable logging carriage, shown in Fig. 8, has been built by the authors. The carriage consists of a main body, and the front and rear carrier modules. The carrier modules employ two skyline pulleys each, arranged in tandem symmetrical around the carrier module pivot points. A standard euro pallet, suspended below the carriage and attached to the carriage via cords, serves as the loading platform for up to 100 kg of payload, made up by four 25 kg weights.

The carriage is suspended on a 12 mm steel cable, serving as the skyline of the miniature setup installed in a forest near Sterzing, Province of Bolzano. The skyline is tensioned between two trees approximately 14 m apart, at a height of about 3 m. The elevation difference across the length of the cableway is approximately 2 m. A 15 mm nylon cable, attached to the front side of the carriages' main body serves as the mainline.

Skyline pretension is regulated by a manual cable hoisting system, and measured by a load cell from PTM s.r.l. (Models AF1 and Advance SP150 of their range of load cells and force reading units), as shown in Figs. 9 and 10, respectively. The load cells' evaluation unit, supplied by an external 12 V lead–acid battery, displays force applied to the cell, with a resolution of 0.2 kg. The measuring range is limited to 250 kg. Since skyline forces of up to 1000 kg were to be expected, a pulley system was employed to multiply the force of the load cell by a factor of four, as visible in Fig. 9.

3.2. Data acquisition and interpretation

The mass of the carriage and the loading platform combined was measured with the help of the load cell, yielding 40.0 kg for m_C. Dimensions D and L are respectively 0.7 m and 0.15 m. The remaining measures required to estimate the skyline force with the proposed approach were read directly from the carriage, as shown in Fig. 11. The carriage was prepared to read β_f and β_r directly from the carrier modules, and α from a plummet mounted on the main body of the carriage.

The setup was used to generate a total of 55 complete sets of data, enabling the comparison of measured (F_{S_M}) and estimated (F_{S_E}) skyline forces. The data, presented in Table 6, is to be interpreted as follows. Since the load cell provides measurements in kg, and since payload mass is defined in steps of 25 kg, all units of force are subsequently given in kg. All measurements taken by the load cell are multiplied by four to account for force multiplication at the pulley system.

Parameter ML indicates the presence of a mainline. For the case ML = "none", there is no mainline attached to the carriage. The carriage therefore moves automatically to the lowest point of the cableway, where its inclination is close to zero. In case ML = "parallel", the carriage is pulled by the mainline close to the upper endpoint of the cableway, which also increases the inclination of the carriages' body. The mainline is oriented in parallel to the skyline, as seen in Fig. 11. This enables approximate mainline force quantification, as well as the quantification of its impact on the setup, without additional measurements.

NLP corresponds to the no-payload pretension of the skyline. That is, F_{S_M} with F_D equal to zero. A total of six different NLP levels were tested. The lowest pretension of 58.4 kg did not allow for the testing without mainline, due to excessive skyline sag leading to ground contact of the loading platform. The remaining five NLP levels were tested under both conditions, with and without the mainline. The data within the brackets in the "parallel" section of the NLP column indicates, to which pretension level the given data responds from the "none" section. It shows that F_{S_M} drops significantly when the carriage moves closer to the endpoint of the cableway, which is to be expected in general.

F_D ranges from 0 kg to 100 kg, corresponding to none to four 25 kg weights being placed on the loading platform. α, β_f and β_r are read from the carriage and given in degrees. F_{S_M} is the skyline force read from the force reading unit, multiplied by four, and also given in kg.

The skyline curvatures (δ_f, δ_r) per pulley on the front and rear carrier modules follow from Eqs. (13) and (14), respectively. F_{S_E} is then given by Eq. (6). FL_{ratio} is the ratio of F_{S_E} and the total load suspended by the skyline, which is the sum of m_C and F_D. Finally, ERR is the percentage error of F_{S_E} with respect to F_{S_M}.

4. Results and discussion

Given the sensitivity of the proposed concept, in particular with respect to measurements of β_f and β_r, it is unreasonable to expect small ERR in this study. The carriage used is hand made, such that an error of a few tenths of a degree in the markings of angle indicators is likely inevitable, in addition to friction and limited symmetry of the carrier modules. In comparison, and as elaborated in Section 2.2, an angle measurement resolution of about 0.04° can be expected with dedicated sensors. Depending on the particular situation, an angle measurement error of only 0.1° can result in an ERR of up to 10%. Force multiplication via the pulley system can also amplify any measurement inaccuracy. That is why the objective of this study is not to determine the accuracy of the proposed approach, but to determine if it is capable of predicting skyline tension.

Results in Table 6 show that ERR is at most 29.5%, while spanning an F_{S_E} range of 62.8 kg to 648.2 kg. The average absolute ERR across

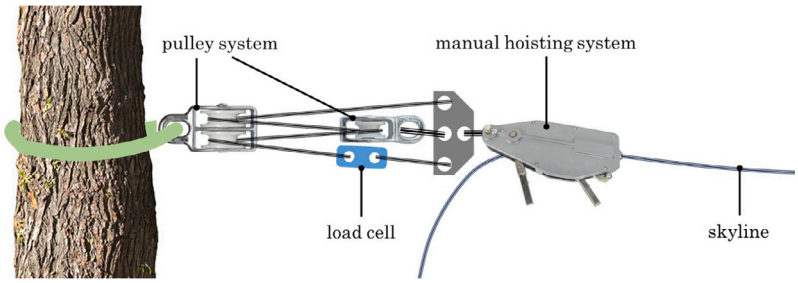

Fig. 9. Setup to pretension the skyline cable and to measure its tensile force with the help of a load cell and pulley system.

Fig. 10. Load cell (a) and force reading unit (b) employed to measure the skyline tensile force during various pretensioning and loading conditions.

Fig. 11. Relative rotation of the carrier modules and carriage inclination read from the carriage.

all 55 datasets is 14.0%. Fig. 12 provides more insights into ERR behavior. F_{S_E} vs. F_{S_M} is plotted on top of each other, with F_{S_M} ordered in rising order. It also provides a plot of the ERR corresponding to the percentage difference of F_{S_E} and F_{S_M}. ERR is mostly scattered within the 5% and 25% range for all measurements.

Fig. 13 shows the relationship between the skyline curvature, F_{S_E} and ERR. Total skyline curvature can be computed by $2 \cdot (\beta_f + \beta_r) = 2 \cdot (\delta_f + \delta_r)$. For better visibility of the trend behavior, individual error data has been averaged with its neighboring error terms. The figure reconfirms that ERR tends to be smaller when F_{S_E} is large, which coincides with skyline curvature being small. ERR also tends to be smaller, when the total skyline curvature is large (large β_f/β_r). This is because in case of large β_f/β_r, FL_{ratio} is small, such that F_{S_E} becomes much less sensitive to angle measurement errors.

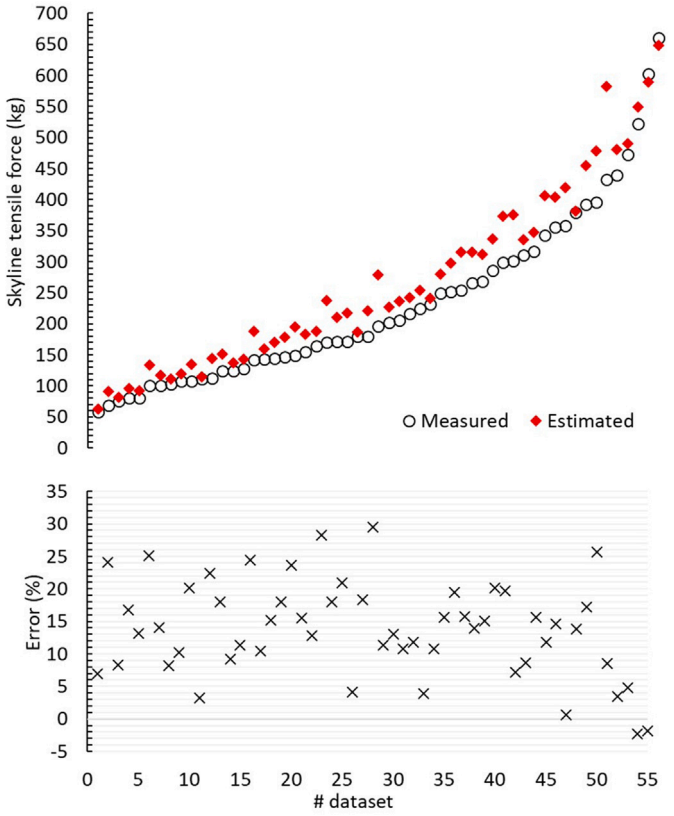

Fig. 12. All 55 sets of F_{S_M} vs. F_{S_E} data plotted on top of each other, with F_{S_M} arranged in rising order (top), and the corresponding ERR with a first order trendline (bottom).

Table 6
Measured vs. estimated skyline tensile forces under various setup conditions (M_L), no-load pretension forces (NLP) and payload (F_D) conditions.

ML	NLP	Measured					Estimated				ERR
[−]	[kg]	F_D [kg]	α [°]	β_f [°]	β_r [°]	F_{S_M} [kg]	δ_f [°]	δ_r [°]	FL_{ratio} [−]	F_{S_E} [kg]	[%]
None	80.0	0	2.5	7.0	5.0	80.0	7.4	4.6	2.4	96.1	16.8
		25	2.5	7.5	5.5	112.0	7.9	5.1	2.2	144.4	22.4
		50	2.8	8.0	5.8	142.4	8.5	5.3	2.1	188.5	24.5
		75	3.0	8.0	6.0	170.4	8.4	5.6	2.1	237.4	28.2
		100	3.5	8.1	6.4	196.8	8.5	6.0	2.0	279.1	29.5
	100.0	0	3.5	5.0	3.6	100.0	5.3	3.3	3.3	133.5	25.1
		25	2.5	5.5	4.1	148.8	5.8	3.8	3.0	194.7	23.6
		50	2.5	5.7	4.5	224.0	6.0	4.2	2.8	253.9	11.8
		75	2.0	6.0	4.6	268.8	6.3	4.3	2.7	312.5	14.0
		100	2.0	6.1	4.7	298.4	6.4	4.4	2.7	373.4	20.1
	127.2	0	3.0	4.5	3.5	127.2	4.7	3.3	3.6	143.5	11.4
		25	2.5	5.0	5.0	179.2	5.0	5.0	2.9	187.0	4.2
		50	2.0	5.0	3.2	265.6	5.4	2.8	3.5	315.4	15.8
		75	2.0	5.2	3.6	301.6	5.5	3.3	3.3	375.7	19.7
		100	2.0	5.6	4.0	358.4	5.9	3.7	3.0	419.6	14.6
	180.0	0	2.0	3.0	2.2	180.0	3.2	2.0	5.5	220.6	18.4
		25	2.0	3.4	2.5	254.4	3.6	2.3	4.9	316.0	19.5
		50	2.0	3.7	2.7	356.0	3.9	2.5	4.5	403.5	11.8
		75	2.0	4.0	2.9	396.0	4.2	2.7	4.2	478.4	17.2
		100	2.0	4.0	2.9	432.8	4.2	2.7	4.2	582.4	25.7
	379.2	0	2.5	1.5	1.5	379.2	1.5	1.5	9.5	381.8	0.7
		25	2.5	2.0	1.8	472.8	2.0	1.8	7.5	489.9	3.5
		50	2.0	2.6	2.1	522.4	2.7	2.0	6.1	548.9	4.8
		75	1.0	3.1	2.5	602.4	3.2	2.4	5.1	589.2	−2.2
		100	0.0	3.5	2.7	660.0	3.7	2.5	4.6	648.2	−1.8
Parallel	68.0 (80.0)	0	15.2	7.0	5.3	68.8	7.4	4.9	2.3	90.6	24.1
		25	14.0	8.0	5.5	108.0	8.5	5.0	2.1	135.2	20.1
		50	13.0	8.9	6.0	144.8	9.5	5.4	1.9	170.7	15.2
		75	13.0	9.0	6.5	172.0	9.5	6.0	1.8	209.8	18.0
		100	12.5	9.3	7.2	231.2	9.7	6.8	1.7	240.7	4.0
	75.2 (100.0)	0	14.0	8.0	5.7	75.2	8.5	5.2	2.0	82.0	8.3
		25	14.0	9.1	6.5	100.8	9.7	5.9	1.8	117.3	14.1
		50	14.0	10.0	6.8	124.0	10.7	6.1	1.7	151.2	18.0
		75	14.0	10.4	7.4	154.4	11.0	6.8	1.6	182.7	15.5
		100	14.0	10.7	7.5	172.0	11.4	6.8	1.6	217.7	21.0
	107.2 (127.2)	0	10.0	4.9	4.6	107.2	5.0	4.5	3.0	119.3	10.2
		25	10.0	5.0	4.8	164.0	5.0	4.8	2.9	188.0	12.8
		50	8.5	5.8	4.8	216.0	6.0	4.6	2.7	242.0	10.7
		75	9.0	6.2	4.8	251.2	6.5	4.5	2.6	297.7	15.6
		100	9.0	6.5	5.0	316.8	6.8	4.7	2.5	346.9	8.7
	111.2 (180.0)	0	12.0	5.0	4.8	111.2	5.0	4.8	2.9	114.9	3.2
		25	11.0	5.5	4.8	146.4	5.6	4.7	2.7	178.4	18.0
		50	10.0	6.0	4.8	205.6	6.3	4.5	2.6	236.5	13.1
		75	9.5	6.8	4.9	249.6	7.2	4.5	2.4	279.8	10.8
		100	9.0	7.0	4.9	311.2	7.4	4.5	2.4	335.4	7.2
	201.6 (379.2)	0	7.8	2.2	2.5	201.6	2.5	2.5	5.7	227.4	11.3
		25	7.5	2.5	2.5	285.6	3.1	2.4	5.2	336.2	15.0
		50	7.5	3.0	2.5	343.2	3.6	2.7	4.5	406.6	15.6
		75	7.5	3.0	2.0	392.0	4.2	3.0	4.0	454.9	13.8
		100	8.0	4.8	3.5	439.2	5.1	3.2	3.4	480.3	8.6
	58.4	0	22.0	10.0	7.2	58.4	10.6	6.6	1.6	62.8	6.9
		25	22.0	11.1	8.0	80.0	11.8	7.3	1.4	92.2	13.2
		50	22.0	12.8	9.2	102.4	13.6	8.4	1.2	111.5	8.2
		75	22.0	13.5	9.5	124.0	14.3	8.7	1.2	136.7	9.3
		100	22.0	14.0	10.0	143.2	14.8	9.2	1.1	159.8	10.4

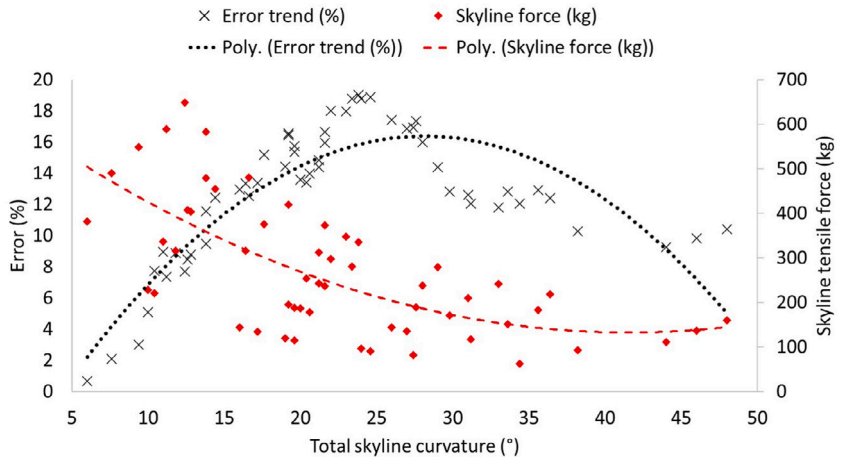

Fig. 13. Relationship between the skyline curvature, F_{S_E} and ERR.

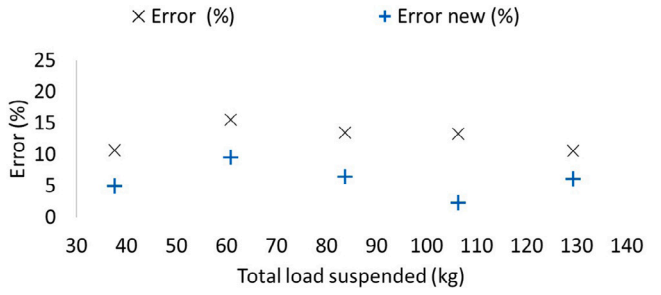

Fig. 14. ERR with (Error) and without (Error new) considering the impact of the mainline force for all 30 datasets in section ML = "parallel".

The results in section ML = "parallel" are in addition influenced by the mainline force. Since the mainline is oriented in parallel to the skyline, as seen in Fig. 11, it has also a vertical component, supporting the suspension of the carriage and payload. While this is accounted for in F_{S_M}, this effect is not considered in the estimation of F_{S_E}, which is thus an overestimation. The force component of the mainline contributing to the suspension of the carriage and payload ($F_{ML_{lift}}$) can be approximated as follows:

$$F_{ML_{lift}} = (m_C + F_D) \cdot sin(\alpha) \cdot tan(2 \cdot \beta_f) \tag{23}$$

The total effective weight suspended by the skyline is thus $m_C + F_D - F_{ML_{lift}}$. A recalculation of F_{S_E} yields the results depicted in Fig. 14. The 30 sets of data from the ML = "parallel" section have been grouped into five datasets, corresponding to the five different loading conditions. Results are plotted with respect to the total effective weight suspended. Their horizontal dislocations from the 40 kg, 65 kg, 90 kg, 115 kg and 140 kg levels indicate the sizes of $F_{ML_{lift}}$. Since F_{S_E} is generally an overestimation, ERR is greatly reduced when considering $F_{ML_{lift}}$, repositioning itself close to the 5% range.

Overall it can be said that while there were inherent sources of inaccuracy in the miniature test setup, results are reasonably accurate and confirm the validity of the proposed approach. Since the anchor points of the skyline were only about 14 m apart, the setup was very stiff. That is, skyline sag due to its own weight was very small. As a consequence, the changes in β_f, β_r and ground clearance of the loading platform due to changes in F_D were very small.

An error in the order of 30% should still render the concept applicable and useful to practical applications. Industry standard skyline force safety factors range between 2.5 and 3.0. Yet still it is not uncommon, that such systems fail. Thus, even if this concept underestimated the actual force by 30%, it would still keep the cableway far from the critical point of failure. What is more, the concept appears to generate mostly overestimations, thus would further prevent skyline overloading.

Further tests are required to capture all effects influencing the result of the proposed approach, and to determine the maximum achievable accuracy. The objective for future work is to equip the self-propelled carriage HULK by Leitalpin (Leitalpin SRL, Bolzano, Italy -www.leitalpin.com) with the sensors required to implement the skyline tensile force observer, as shown in Fig. 15 Arch sensors are installed in both tandem carrier modules to measure β_f and β_r up to a few hundredths of degrees of accuracy, while a load shaft directly measures F_{Cy_r} at one of the skyline pulleys of the rear carrier module. Data processing is performed within the carriage and F_{S_E} can be read in real time from the remote controller. The remote controller also provides the interface to set skyline force limits not to be exceeded during lateral yarding and inhauling.

5. Conclusion

Excessive forces on skylines and tail spars are the frequent cause of severe and destructive accidents in cable logging. Existing force monitoring and limiting solutions are only partially effective. To address this challenge, a skyline tensile force observer concept was developed and tested in this work. The concept to be implemented in cable logging carriages enables the estimation of the skyline force in real-time, based on a few measurements within the carriage itself. As a consequence, winch pull and traction force can be dynamically limited to ensure adequate skyline safety factors. The continuous skyline load profile can also serve as an input to cable predictive maintenance models. The concept was tested with the help of a small scale test setup. Measured and predicted skyline forces differed by at most 29%, whereas the mean absolute error was 14% among a total of 55 measurements. This mismatch can in part be attributed to the limited accuracy of manually taken measurements. The solution proved feasible for applications in any type of cable logging carriages. More generally, any equipment suspended by tensioned cables can make use of these principles. In a future study, the skyline force observer will be implemented in the self-propelled carriage HULK. Measurements will be taken by high resolution sensors, and predicted and measured force trajectories will be recorded by data loggers for long-term performance evaluations.

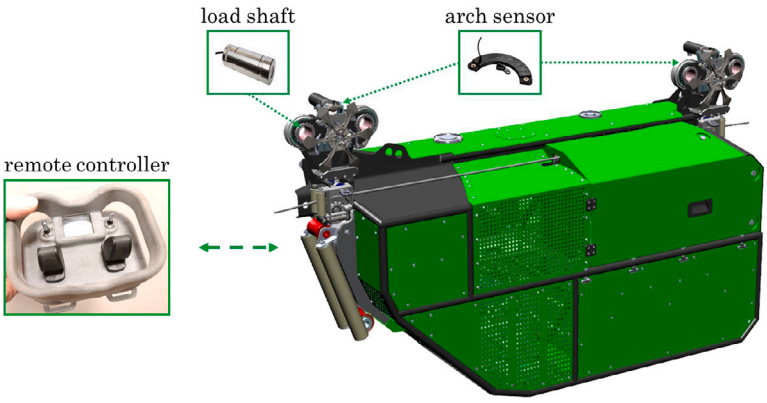

Fig. 15. Sensors installed into the self-propelled carriage HULK to equip it with the skyline tensile force observer.

Funding

This study was carried out within the Agritech National Research Center (Task 4.1.4) and received funding from the European Union Next-GenerationEU (PIANO NAZIONALE DI RIPRESA E RESILIENZA (PNRR) – MISSIONE 4 COMPONENTE 2, INVESTIMENTO 1.4 – D.D. 1032 17/06/2022, CN00000022).

CRediT authorship contribution statement

Stefan Leitner: Conceptualization, Investigation, Methodology, Validation, Writing – original draft, Writing – review & editing. **Giovanni Carabin:** Supervision, Writing – review & editing. **Raffaele Spinelli:** Supervision, Writing – review & editing. **Massimiliano Renzi:** Supervision, Writing – review & editing. **Renato Vidoni:** Funding acquisition, Methodology, Supervision, Writing – review & editing.

Declaration of competing interest

The authors declare the following financial interests/personal relationships which may be considered as potential competing interests: Renato Vidoni reports financial support was provided by European Union Next-GenerationEU. Leitner Stefan reports a relationship with LeitAlpin that includes: equity or stocks. If there are other authors, they declare that they have no known competing financial interests or personal relationships that could have appeared to influence the work reported in this paper.

Data availability

Data will be made available on request.

References

[1] B. Talbot, K. Stampfer, R. Visser, Machine function integration and its effect on the performance of a timber yarding and processing operation, Biosyst. Eng. 135 (2015) 10–20.
[2] P.M. Albizu-Urionabarrenetxea, E. Tolosana-Esteban, E. Roman-Jordan, Safety and health in forest harvesting operations. Diagnosis and preventive actions. A review, For. Syst. 22 (3) (2013) 392–400.
[3] T. Varch, G. Erber, R. Visser, R. Spinelli, H. Harrill, K. Stampfer, Advances in cable yarding: A review of recent developments in skyline carriage technology, Curr. For. Rep. 7 (4) (2021) 181–194.
[4] J. Klun, M. Medved, Fatal accidents in forestry in some European countries, Croat. J. For. Eng. 28 (1) (2007) 55–62.
[5] M. Allman, M. Jankovský, Z. Allmanová, M. Ferenčík, V. Messingerová, M. Vlčková, S. Stoilov, Work accidents during cable yarding operations in central europe 2006 – 2014, For. Syst. 26 (1) (2017).
[6] P.A. Tsioras, C. Rottensteiner, K. Stampfer, Analysis of accidents during cable yarding operations in Austria 1998–2008, Croat. J. For. Eng. 32 (2) (2011) 549–560.
[7] L. Marchi, O. Mologni, D. Trutalli, R. Scotta, R. Cavalli, L. Montecchio, S. Grigolato, Safety assessment of trees used as anchors in cable-supported tree harvesting based on experimental observations, Biosyst. Eng. 186 (2019) 71–82.
[8] L. Marchi, D. Trutalli, O. Mologni, R. Gallo, D. Roeser, R. Cavalli, S. Grigolato, Mechanical response of natural anchors in cable logging, Int. J. For. Eng. 32 (1) (2021) 29–42.
[9] L. Marchi, O. Mologni, S. Grigolato, R. Cavalli, Evaluation on the stability of tree used as anchors in cable yarding operations: A preliminary test based on low-cost MEMS sensors, in: Lecture Notes in Civil Engineering, vol. 67, 2020, pp. 473–479.
[10] S. Dupire, F. Bourrier, F. Berger, Predicting load path and tensile forces during cable yarding operations on steep terrain, J. For. Res. 21 (1) (2016) 1–14.
[11] O. Mologni, L. Marchi, C.K. Lyons, S. Grigolato, R. Cavalli, D. Röser, Skyline tensile forces in cable logging: Field observations vs. software calculations, Croat. J. For. Eng. 42 (2) (2021) 227–243.
[12] O. Mologni, C.K. Lyons, G. Zambon, A.R. Proto, G. Zimbalatti, R. Cavalli, S. Grigolato, Skyline tensile force monitoring of mobile tower yarders operating in the Italian Alps, Eur. J. For. Res. 138 (5) (2019) 847–862.
[13] Z. Ma, J. Choi, H. Sohn, Noncontact cable tension force estimation using an integrated vision and inertial measurement system, Measurement 199 (2022) 111532.
[14] G. Wang, W. Lu, C. Yuan, Y. Wang, P. Zhang, Y. Fan, Q. Kong, A vision-based method for estimating shallow cable tension via vibrational properties, Measurement 195 (2022) 111070.
[15] Z. Yu, S. Shao, N. Liu, Z. Zhou, L. Feng, P. Du, J. Tang, Cable tension identification based on near field radiated acoustic pressure signal, Measurement 178 (2021) 109354.
[16] J. Weng, L. Chen, L. Sun, Y. Zou, Z. Liu, H. Guo, Fully automated and non-contact force identification of bridge cables using microwave remote sensing, Measurement 209 (2023) 112508.